Oxygen *K*-edge XANES of germanates investigated using first-principles calculations

Delphine Cabaret and Francesco Mauri*

*Institut de Minéralogie et de Physique des Milieux Condensés, UMR CNRS 7590, Université Pierre et Marie Curie, Paris 6,
140 rue de Lourmel, F-75015 Paris, France*

Grant S. Henderson†

Department of Geology, University of Toronto, 22 Russell Street, Toronto, Ontario M5S 3B1, Canada
(Received 4 October 2006; published 17 May 2007)

O *K*-edge x-ray absorption near-edge structure (XANES) spectra of α-quartz-type and rutile-type GeO$_2$ polymorphs and of K$_2$Ge$_8$O$_{17}$ have been analyzed using first-principles plane-wave pseudopotential calculations. XANES spectra have been calculated using supercell including core-hole effects and good agreement with experiment has been obtained. In the the case of GeO$_2$ polymorphs, local density of empty states has been performed and peaks in the experimental spectra can be assigned to transitions involving hybridization of the O *p* orbitals with the Ge *s*, Ge *p*, Ge *sp*, and Ge *d* orbitals. Furthermore, peak positions in the theoretical spectra appear to be correlated with changes in the Ge-O-Ge angle as well as indirectly with the Ge coordination geometry. Analysis of O *K*-edge XANES spectra for individual O sites in K$_2$Ge$_8$O$_{17}$ shows that oxygens shared between two fivefold Ge atoms or one fourfold and one fivefold Ge atom exhibit subtle shifts to lower energy of the peaks, which have been previously observed in alkali germanate glasses at and above the germanate anomaly.

DOI: 10.1103/PhysRevB.75.184205   PACS number(s): 61.10.Ht, 61.82.Ms, 71.20.$-$b

I. INTRODUCTION

Alkali containing germanate glasses exhibit a phenomenon widely known as the "germanate anomaly."[1] Physical properties such as density or refractive index exhibit a dependence on the alkali content in these glasses. In the case of density, there is a density increase with addition of alkali which reaches a maximum that is alkali dependent, followed by a decline in density with continued addition of alkali. The traditional mechanism for explaining the germanate anomaly in alkali germanate glasses which remains widely accepted is a change from fourfold to sixfold coordination of germanium (Ge).[2,3] The coordination change hypothesis suggests that the density increase is due to the formation of sixfold Ge without the formation of nonbridging oxygens (NBOs), while the density decrease is due to the conversion of sixfold Ge back to fourfold Ge with the formation of NBOs.[1] An alternative hypothesis involving small ring formation, which does not involve the formation of sixfold Ge, was proposed in Ref. 2 and expanded upon in Ref. 3. However, the coordination change hypothesis remains widely accepted, despite the inconsistencies pointed out in Ref. 3 and understanding the atomistic mechanism of the germanate anomaly remains an important issue in the physical chemistry of glasses.

More recently, fivefold Ge has been suggested as a potential coordination involved in the anomaly.[4–6] However, the techniques used to identify higher-coordinated species (extended x-ray absorption fine structure, neutron scattering, and x-ray scattering) have not been successful in being able to discriminate between different coordination geometries in these glasses (see Refs. 6–8 for a more detailed discussion). In general, they merely determine, with the addition of alkali, the existence of a population of lengthened Ge-O bonds and these lengthened Ge-O bonds are attributed to the presence of a higher-coordinated Ge environment. This inability to clearly discriminate a change in the Ge coordination arises

because in these glasses, less than 20% of the Ge atoms are believed to undergo a coordination change. These techniques have been more successful when investigating glasses at pressure where most, if not all, the fourfold Ge atoms convert to fivefold or sixfold coordination (e.g., see Ref. 9).

Recently, O *K*-edge x-ray absorption near-edge structure (XANES) spectroscopy has been shown to be sensitive to the coordination environment of the cation bound to the oxygen.[10] Consequently, the O *K* edge is potentially a useful probe of the Ge environment. Using O *K*-edge spectra of trigonal GeO$_2$ (fourfold Ge with α-quartz-like structure), tetragonal GeO$_2$ (sixfold Ge with rutile-type structure), and K$_2$Ge$_8$O$_{17}$ (fourfold and fivefold Ge) as model compounds for different Ge environments, it was shown in Ref. 11 that the O *K*-edge spectra for each of the model compounds exhibit distinct spectral features which can be used as structural fingerprints for comparing the O *K*-edge spectra of the alkali glasses. It was found that the XANES spectra of the alkali germanate glasses do show the presence of fivefold Ge with the addition of alkali oxide to the glass structure.[11] However, the composition at which this species occurs depends on the size of the alkali cation: Li-containing germanates do not contain any appreciable amount of fivefold Ge; Na- and K-bearing germanate glasses have fivefold Ge at the anomaly maximum and beyond, while the XANES spectra of the Rb- and Cs-bearing glasses show that there is onset of fivefold Ge formation almost immediately upon addition of these alkalis. However, the authors of Ref. 11 also found that the presence of fivefold Ge is associated with the formation of NBOs and is not important for the density behavior.[12]

Clearly, O *K*-edge XANES is a useful technique for elucidating the Ge coordination geometry in alkali-germanate glasses. However, without numerical simulation and detailed analysis of the electronic transitions contributing to the experimental spectra, the use of O *K*-edge XANES for determining Ge coordination environments must remain some-

what qualitative. Here, we provide the first results of detailed first-principles numerical simulations of the O K-edge spectra for the model compounds employed in the studies of Refs. 11 and 12: the two GeO_2 polymorphs, with α-quartz-like structure and with rutile-type structure, called $q-GeO_2$ and $r-GeO_2$, respectively, as well as $K_2Ge_8O_{17}$ which has germanium in differing coordination environments and oxygen in eleven nonequivalent crystallographic sites. The experimental spectra are analyzed using XANES absorption cross section and local density of states (DOS) calculations. All the calculations are performed using a framework based on density-functional theory (DFT) in the local-density approximation (LDA), with plane-wave basis set and pseudopotentials. The derivation of the absorption cross section within such a formalism is described in Refs. 13 and 14.

The paper is organized as follows. Section II summarizes the experimental details of the O K-edge XANES experiments. Section III describes the crystallographic structures of the model compounds and gives the calculation parameters of both the XANES and local DOS calculations. Section IV is devoted to the results and discussion and is divided in three parts. First, a comparison between experimental and calculated spectra is made (Sec. IV A). Second, after an evaluation of the core-hole effects, the spectral features of the O K-edge XANES spectra of the GeO_2 polymorphs are analyzed using local DOS calculations and compared with the O K-edge spectra of the corresponding SiO_2 polymorphs (Sec. IV B). Third, using the results of Sec. IV B, the spectral features of the O K-edge XANES spectrum of $K_2Ge_8O_{17}$ are assigned to specific arrangements around the oxygen atoms in terms of Ge-O-Ge angles and of Ge coordination (Sec. IV C). Conclusions are given in Sec. V.

II. EXPERIMENTS

The experimental O K-edge XANES spectra were obtained on the samples described in Refs. 3 and 11. The O K-edge spectra were recorded at the Canadian Synchrotron Radiation Facility (CSRF), Aladdin 1 GeV storage ring, University of Wisconsin at Madison using the spherical grating monochromator (SGM) beamline. In addition, some spectra were also recorded on the SGM beamline at the Canadian Light Source (CLS) at Saskatoon. Beam conditions and experimental details for CSRF are given in Ref. 11. The beamline at CLS has three gratings with line spacings of 600, 1100, and 1700 lines/mm which extend the photon region from 250 to 2000 eV. The energy resolution is approximately 0.05 eV at the O K edge. The photon flux at 100 mA is 1012 photons/s and the beam size is greater than 1 mm (horizontal) $\times 100$ μm (vertical).[15]

III. CALCULATIONS

A. Model compounds

The starting point of the XANES first-principles calculations is a structural model. For this study, the starting structures are $q-GeO_2$, $r-GeO_2$, and $K_2Ge_8O_{17}$. Crystalline GeO_2 exists at ambient temperatures and pressures as one of two polymorphs: an α-quartz-like ($P3_221$) trigonal structure

with hexagonal unit cell[16,17] or as a rutile-type tetragonal ($P4_2/mnm$) structure.[18] The α-quartz-like GeO_2 structure is actually the stable high-temperature phase.[19] While the structure is very similar to that of α-quartz, there are differences: the GeO_4 tetrahedra are more distorted due to greater variation in the O-Ge-O angles within the tetrahedron which range from 106.3° to 113.1° with a Ge-O-Ge angle of 130.0°. Both the Ge and O atoms each occupy single sites within the unit cell. The rutile GeO_2 polymorph, which transforms to the α-quartz-like structure at 1281 K (cf., Refs. 19 and 20 and references therein), has a structure similar to that of stishovite[18] and like the α-quartz-like polymorph, Ge and O each occupy only one unique site within the structure. Within the GeO_6 octahedron, the two axial bonds are longer than the four equatorial Ge-O bonds: 1.902±0.001 and 1.872±0.001 Å, respectively. In contrast, the two independent Ge-O distances in the α-quartz-like GeO_2 structure are similar at 1.737±0.003 and 1.741±0.002 Å.[17] A detailed review of the structure and behavior of GeO_2 polymorphs is given in Ref. 8.

The structure of $K_2Ge_8O_{17}$ is orthorhombic ($Pnma$) and is similar to a feldspar structure.[21,22] It contains four distinct germanium sites and 11 oxygen sites within the unit cell. Of the four Ge sites, one is in fivefold coordination and the other three are in tetrahedral coordination. The fivefold Ge site has a distorted trigonal bipyramid geometry with one of the oxygens (O4) pointing into the center of the small four-membered rings (Fig. 1). This oxygen along with another (O1) is shared with adjacent fivefold Ge atoms in an edge sharing arrangement. The edge sharing GeO_5 polyhedral pairs are parallel to the b axis. When viewed down [010], the framework structure consists of four- (composed of three GeO_4 and one GeO_5 groups) and eight-membered (composed of six GeO_4 and two GeO_5 groups) rings of Ge polyhedra (Fig. 1): the K atoms sit within the eight-membered Ge rings.

B. Computational details

The XANES calculations are performed within a first-principles total-energy code[41] using the formalism described in Refs. 13 and 14. The method based on DFT-LDA uses plane-wave basis sets, norm-conserving pseudopotentials[23] in the Kleinman-Bylander form,[24] and periodic boundary conditions. The 1s core hole is taken into account within a supercell that has to be large enough to avoid interaction between absorbing atoms belonging to neighboring cells. The calculation is carried out in two steps: (i) the determination of a self-consistent potential for the supercell including the 1s core hole and (ii) the computation of the cross section as a continued fraction following the numerical method described in Refs. 25 and 26. The absorption cross section is calculated beyond the "muffin-tin" approximation; the latter is a known limitation for the application of multiple scattering theory traditionally used for XANES simulations. The all-electron final-state wave function of the absorbing atom is reconstructed using two p projectors within the projector augmented wave method.[27]

The parametrization used for the generation of the pseudopotentials is given in Table I. The pseudopotential of
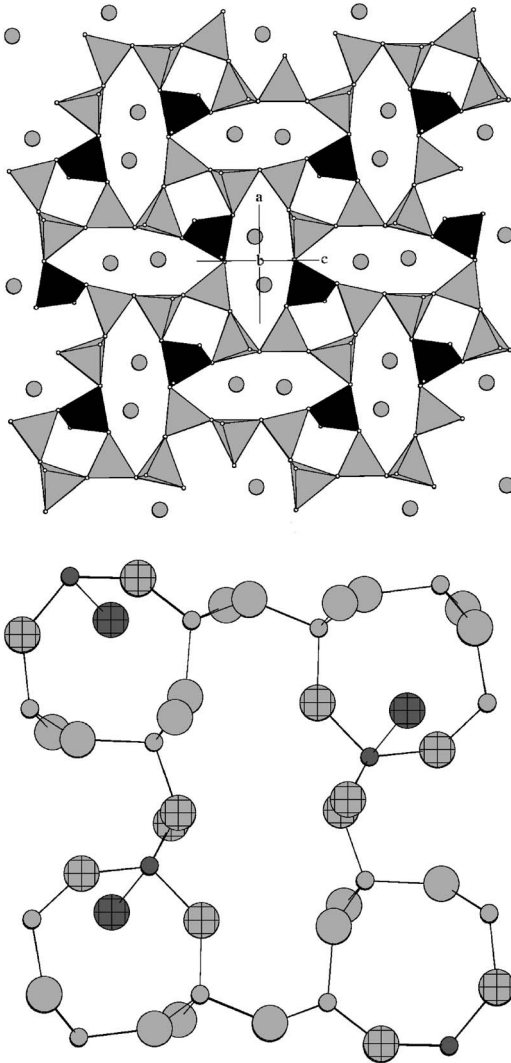
FIG. 1. Top: structure of $K_2Ge_8O_{17}$ viewed down [010]. The K atoms (gray circles) occupy the eight-membered rings made up of six GeO_4 tetrahedra (gray) and two GeO_5 polyhedra (black), Bottom: "ball and stick" representation of the structure. Oxygens associated with the fivefold Ge are in gray (cross hatched), those with the fourfold Ge in gray, and the oxygens in the trigonal bipyramid that are shared are in dark gray (cross hatched). K atoms have been deleted for clarity.

potassium includes nonlinear core corrections. The pseudopotential of the oxygen absorbing atom is obtained by considering only one 1*s* electron on the oxygen electronic configuration. The absorbing atom is isolated in a $2 \times 2 \times 2$ supercell for *q*-GeO_2 (i.e., 72 atoms), a $2 \times 2 \times 3$ supercell for *r*-GeO_2 (i.e., 72 atoms), and a $1 \times 1 \times 1$ supercell for $K_2Ge_8O_{17}$ (i.e., 108 atoms), built from the crystal structures given in Refs. 18, 22, and 28, respectively. Convergence of the XANES theoretical spectra is reached for the following set of parameters: a 70 Ry energy cutoff for the plane-wave expansion, one *k* point for the self-consistent electronic potential calculation, and $3 \times 3 \times 3$ *k*-point grid (*q*- and *r*-GeO_2) and $2 \times 2 \times 2$ *k*-point grid ($K_2Ge_8O_{17}$) for the absorption cross-section calculation. A constant broadening pa-

TABLE I. Parametrization used for the generation of the pseudopotentials. The core radii of the valence states are indicated in parentheses in Å.

Atom	Ge	O	O (core hole)	K
Valence states	$4s^2$ (0.90)	$2s^2$ (0.77)	$2s^2$ (0.74)	$3s^2$ (0.63)
	$4p^{1.8}$ (1.11)	$2p^4$ (0.77)	$2p^4$ (0.74)	$3p^6$ (0.69)
	$4d^{0.2}$ (1.59)		$3d^0$ (0.74)	$3d^0$ (0.84)
Local part	s	p	d	s

rameter (0.5 eV) is used in the continued fraction.

In *q*- and *r*-GeO_2, oxygen atoms occupy single crystallographic sites, while the crystal structure of $K_2Ge_8O_{17}$ contains 11 distinct oxygen atomic sites. Consequently, for $K_2Ge_8O_{17}$, 11 calculations have been carried out, and the resulting theoretical O *K*-edge spectrum is the weighted average of 11 individual contributions according to the multiplicity of each oxygen atomic site. At each inequivalent site, the *K*-edge energy (the energy required to promote the core 1*s* electron to the conduction-band minimum) is different, because both the 1*s* energy and the conduction-band edge, in the presence of the core hole, are site dependent. To align the XANES theoretical spectra of inequivalent sites (of the same or of different compounds), we take into account the site-dependent 1*s* energy by subtracting from the energies of the conduction states the Kohn-Sham potential, $V_{KS}(\mathbf{r})$, averaged on the 1*s* core region,

$$\langle V_{KS} \rangle = \int V_{KS}(\boldsymbol{r})\rho(\boldsymbol{r})d^3r, \qquad (1)$$

where $\rho(\boldsymbol{r}) = 0$ outside the core region and $\int \rho(\boldsymbol{r})d^3r = 1$. In Eq. (1), the Kohn-Sham potential has been determined for the supercell including the core hole. Since the variation of $V_{KS}(\boldsymbol{r})$ from one site to another is smooth and uniform in the core region, the variation of $\langle V_{KS} \rangle$ from one site to another does not depend on the function $\rho(\boldsymbol{r})$. Here, $\rho(\boldsymbol{r})$ is chosen as

$$\rho(\boldsymbol{r}) = \frac{|\langle \boldsymbol{r} | \widetilde{p_{2s}} \rangle|^2}{\int |\langle \boldsymbol{r} | \widetilde{p_{2s}} \rangle|^2 d^3r}, \qquad (2)$$

where the projector function $|\widetilde{p_{2s}}\rangle$ is defined in Eq. (4) of Ref. 13.

The local DOS calculations were performed using the same first-principles total-energy code as that used for the XANES calculations. They were carried out on unit cells of *q*-GeO_2 and *r*-GeO_2, with an energy cutoff of 70 Ry. The crystal wave function was decomposed into different angular momentum channels within spheres of 0.77 and 1.11 Å radii centered on O and Ge atoms, respectively. The self-consistent electronic potential was determined using $4 \times 4 \times 6$ and $4 \times 4 \times 4$ Monkhorst-Pack *k*-point grids for *q*-GeO_2 and *r*-GeO_2, respectively.[29] The DOS were evaluated using $8 \times 8 \times 12$ and $8 \times 8 \times 6$ Monkhorst-Pack *k*-point grids for
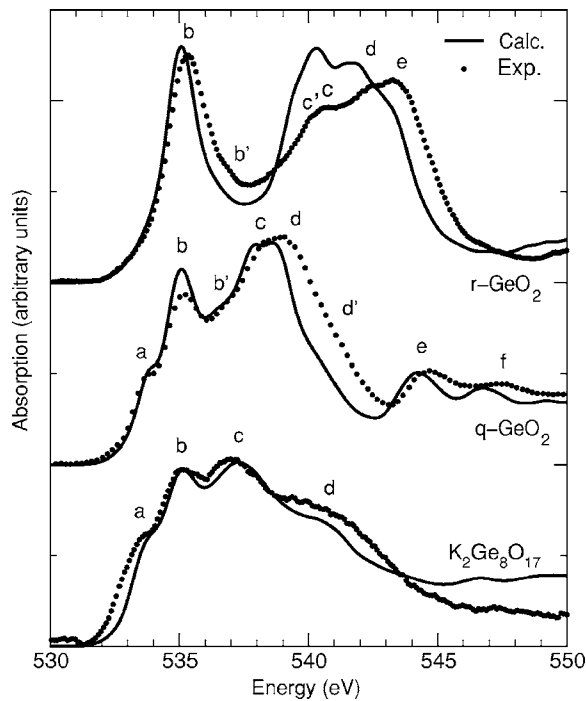
FIG. 2. Comparison of the calculated (solid curves) and experimental (dotted curves) O K-edge XANES spectra of α-quartz-like (q-GeO$_2$) and rutile-type (r-GeO$_2$) GeO$_2$ polymorphs and for the K$_2$Ge$_8$O$_{17}$ structure.

q-GeO$_2$ and r-GeO$_2$, respectively. The local DOS were convoluted with a Gaussian broadening function with a full width at half maximum of 0.3 eV.

IV. RESULTS AND DISCUSSION

A. Comparison between experimental and theoretical spectra

The calculated and experimental O K-edge spectra for the α-quartz-like (q-GeO$_2$) and rutile-type (r-GeO$_2$) GeO$_2$ polymorphs and that of K$_2$Ge$_8$O$_{17}$ are shown in Fig. 2. The three calculated spectra have been shifted by the same quantity to match with experiment. The O K-edge XANES spectrum of r-GeO$_2$ exhibits a well-defined peak at 535.3 eV (peak b) with a small shoulder at $\sim$536.9 eV (peak b$'$) and a further set of three features at 540.6 (peak c), 542.4 (peak d), and 543.2 eV (peak e). A small shoulder on peak c, labeled c$'$, can be distinguished at $\sim$540.0 eV. The calculated spectrum is in good agreement with the experimental one. The strong absorption peak at 535.3 eV in the experimental spectrum is reproduced well by the calculation. Furthermore, the position of the peaks c$'$, c, and e are also comparable, although their relative intensities are reversed in the calculated spectrum. Peak d is at lower energy in the simulated spectrum by 0.6 eV.

The O K-edge XANES spectrum of q-GeO$_2$ is distinct from that of r-GeO$_2$. The spectrum of the α-quartz-like GeO$_2$ polymorph reveals eight features in the energy range of 530–550 eV: a shoulder at $\sim$533.8 eV (peak a), a distinct peak at 535.2 eV (peak b), a small shoulder at $\sim$536.6 eV (peak b$'$), a more intense double feature at 538.2 and 539 eV

(peaks c and d, respectively), a very weak shoulder d$'$ around 541 eV, and two relatively sharp but weaker peaks at 544.6 eV (peak e) and 547.4 eV (peak f). Comparison of the calculated XANES spectrum of the q-GeO$_2$ polymorph with that obtained experimentally shows that the calculation reproduces the position and intensity of all the experimentally observed peaks quite well. The principal difference is that from 537 eV onward, the calculated peaks are at lower energy as compared to experiment. This point is often observed in XANES calculations performed within LDA, which is known to underestimate band gaps and conduction-band energies.

The K$_2$Ge$_8$O$_{17}$ O K-edge XANES spectrum is more similar to that of the q-GeO$_2$ than to that of the r-GeO$_2$ polymorph. It exhibits three main peaks at 533.7 eV (peak a), 535.1 eV (peak b), and 537.2 eV (peak c). Peaks a and b are at the same energy (within experimental error) as peaks a and b of the q-GeO$_2$ polymorph. However, peak c is shifted to lower energy and the broad peak d is located at the same energy as the shoulder d$'$ of q-GeO$_2$. The simulated XANES spectrum of K$_2$Ge$_8$O$_{17}$ also reproduces very well the position and intensities of the experimentally observed XANES spectrum.

B. Core-hole effects and local density of states calculations of r-GeO$_2$ and q-GeO$_2$

In order to understand the origin of the spectral features of r-GeO$_2$ and q-GeO$_2$ from an electronic perspective, the core-hole effects were investigated and the local DOSs were calculated (see Figs. 3 and 4). The latter allows assignment of the peaks in terms of hybrization between O and Ge empty orbitals.

The upper panels of Figs. 3 and 4 (panels a) show the core-hole effects in the calculated O K-edge XANES spectra in r-GeO$_2$ and q-GeO$_2$, respectively. Indeed, the core-hole-included supercell cross-section calculations are compared with unit cell cross-section calculations obtained without any core hole on the oxygen absorbing atom. For both polymorphs, the presence of the core-hole creates an attractive potential that shifts the features toward lower energy. When the core hole is present, the intensity of the first main features (b for r-GeO$_2$ and a and b for q-GeO$_2$) is increased, while the intensity of the higher-energy peaks (d and e for r-GeO$_2$ and c and d for q-GeO$_2$) is drastically decreased.

In the case of r-GeO$_2$, the relative intensities of the set of peaks c$'$, c, d, and e are more consistent with the experimental spectrum (Fig. 2) when the core hole is not taken into account than when it is included within the supercell calculation. This suggests that the core-hole potential is too attractive in the supercell calculation: the screening by the valence electrons is not completely satisfactorily modeled in the r-GeO$_2$ case by using the supercell approach. This has already been observed at the Al K-edge in corundum (α-Al$_2$O$_3$).[14] This problem is often attributed to the fact that a full core hole may overestimate the core-hole effects.[30,31]

Although the core-hole effects have to be taken into account to provide good agreement with experiment, the calculations without core hole do exhibit all the experimental
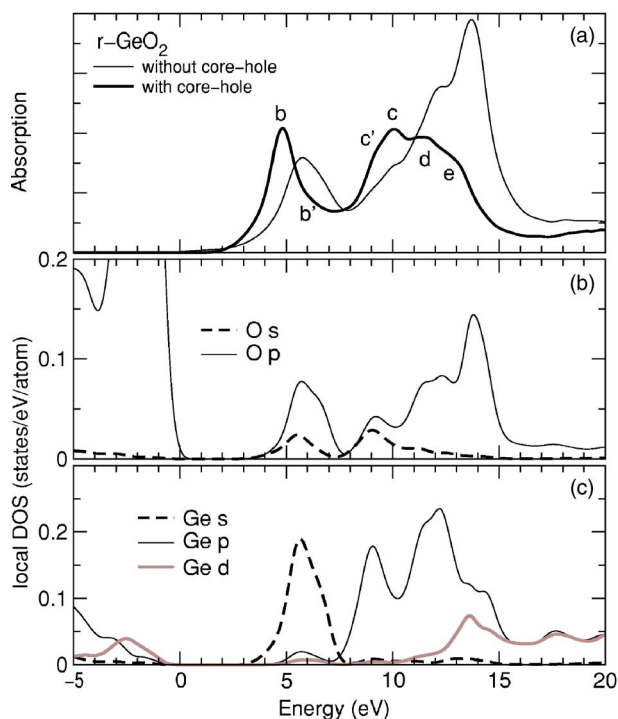
FIG. 3. (Color online) Theoretical O K-edge spectra calculated with and without core hole compared with (a) local DOS of r-GeO$_2$ (rutile-type polymorph), (b) s and p local DOSs of oxygen atoms, and (c) s, p, and d local DOSs of germanium atoms.
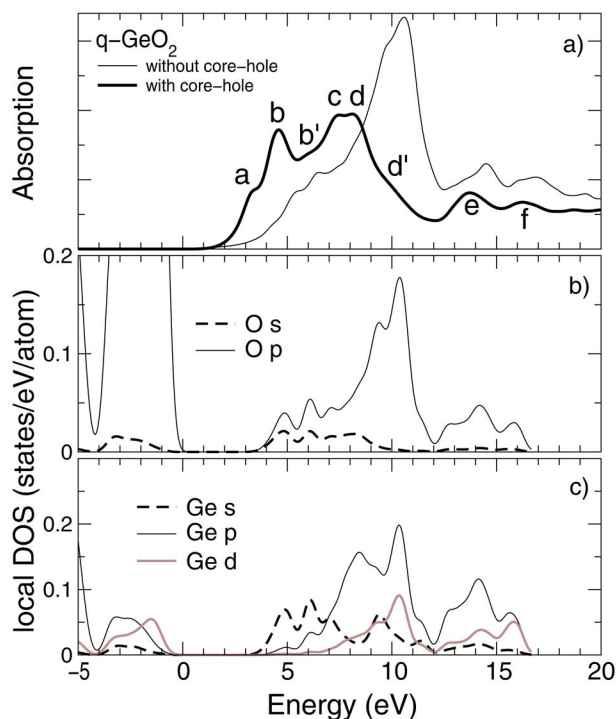

FIG. 4. (Color online) Theoretical O K-edge spectra calculated with and without core hole compared with (a) local DOS of q-GeO$_2$ (quartz-type polymorph), (b) s and p local DOSs of oxygen atoms, and (c) s, p, and d local DOSs of germanium atoms.

features with relative energy positions that are consistent with the experimental spectra. This means that ground-state calculations, such as DOS calculations, provide useful information to interpret the features in terms of orbital hybridizations.[32,33] The total DOSs have been compared with similar calculations in the literature (using plane-wave pseudopotential within DFT-LDA). Our results are in good agreement with the calculations of Ref. 34, except for the empty states of q-GeO$_2$. In Ref. 34, larger core radii than ours were used for the generation of the Ge and O pseudopotentials. Nevertheless, our q-GeO$_2$ occupied and empty DOS calculations are in total agreement with that of Ref. 35.

Panels (b) and (c) of Figs. 3 (r-GeO$_2$) and 4 (q-GeO$_2$) show the local DOS of O and Ge, respectively. For both compounds, the empty O states are mainly p states. One can notice that the O p empty DOS are very similar to electric dipole cross sections obtained without core hole (the main difference resulting from a different broadening parameter). Indeed, since the local DOSs were computed using small projection radii, the radial dipole matrix elements are not energy dependent. This point has also been mentioned in the case of Si and O K edges and the corresponding Si p and O p local DOSs in α-quartz.[13] In the case of r-GeO$_2$ polymorph, the Ge empty local DOSs are characterized by an intense Ge s peak in the first 4 eV of the conduction band, followed by first a set of Ge p intense peaks, and then Ge d states. Consequently, Fig. 3 shows that the sharp peak (peak b) of the XANES spectrum result from hybridization between O p states and Ge s states, peaks c′, c, and d, from hybridization between O p states and Ge p states and that peak e is due to

hybridization between O p and Ge p/d states. In the case of the q-GeO$_2$ polymorph, the situation is not much different. The main difference concerns the shape of the Ge s states that are more extended, showing the sp hybrid character of Ge-O bond in the compound. Peak a appears to be mainly due to hybridization of O p states with Ge s states, peak b is due to hybridization of O p and Ge sp states, peaks b′ and c are mainly related to hybridization between O p and Ge p states, and peaks d and d′ result from hybridization involving both Ge sp and d states.

The r-GeO$_2$ and q-GeO$_2$ polymorphs are isostructural to stishovite and α-quartz, respectively. One would expect the O K-edge spectra, as well as the electronic properties, to be comparable to those of the SiO$_2$ polymorphs. The calculated[36] and experimental[37] spectra of stishovite are indeed similar to those of r-GeO$_2$ (Fig. 2): in both compounds, the sharp peak (peak b) followed by a set of features extending over an ~7 eV energy range are observed.

However, the case of α-quartz and q-GeO$_2$ is surprisingly different. The O K-edge calculated and experimental spectra of α-quartz strongly differ from those of q-GeO$_2$ in the first three eV energy range (cf. Refs. 13, 36, and 38). Peak a is not present in the O K-edge spectrum of α-quartz and peak b is a small preedge peak of feature c. In addition, Tamura *et al.*[35] noticed some discrepancies in the top of the valence band and in the bottom of the conduction band between α-quartz and q-GeO$_2$. The authors attributed these differences to the fact that the O-O distances are longer in q-GeO$_2$ than in α-SiO$_2$. Indeed, the O-O distances are increased by ~6.5% and 9% between α-quartz and q-GeO$_2$ (see Table II

TABLE II. Experimental structural parameters of α-quartz, q-GeO$_2$, stishovite, and r-GeO$_2$.

	α-quartz-type compounds		Rutile-type compounds	
	α-quartz[a]	q-GeO$_2$[b]	Stishovite[c]	r-GeO$_2$[d]
Cell parameters	a=4.912 Å	a=4.985 Å	a=4.181 Å	a=4.395 Å
	c=5.404 Å	c=5.648 Å	c=2.666 Å	c=2.860 Å
Cation-O bond length (Å)	1.61	1.74	1.76	1.87
			1.81	1.91
O-O distance (Å)	2.61	2.78	2.29	2.40
	2.64	2.90	2.52	2.67
			2.66	2.86
Cation-O-cation angle (deg)	143.7	130.0	98.7	100.0
			130.7	130.0

[a]From Ref. 40.
[b]From Ref. 28.
[c]From Ref. 20.
[d]From Ref. 18.

where we report the cell parameters, interatomic distances, and angles of the four compounds). However, the O-O distances are also greater in r-GeO$_2$ than in stishovite (of about 4.8%, 6%, and 7.5%). Therefore, according to the interpretation given by Tamura *et al.*,[35] one should expect some important differences in the empty DOS and in the O K-edge spectra in the rutile-type compounds too, but this is not the case. The differences between the O K-edge spectra of α-quartz and q-GeO$_2$ are due to a difference in Ge and O local empty states: the overlap between O p and Ge s states is more extended in q-GeO$_2$ than in α-quartz. This is corroborated by the study of Garvie *et al.*[38] Their unoccupied local DOS calculations carried out on α-quartz do show that the Ge p states are more important than the Ge s states 1 eV above the bottom of the conduction band, while the Ge s states dominate the Ge p states over a 3 eV energy range in q-GeO$_2$ (Fig. 4). This difference in the hybridization between O p states and Ge s states between the two compounds is related to the strong differences in angles within the tetrahedra: the Si-O-Si angle is 143.7° in α-quartz, while the Ge-O-Ge angle is only 130° in q-GeO$_2$ (cf. Table II). In the rutile-type compounds, the O K-edge spectra are comparable, and the Si-O-Si and Ge-O-Ge angles are very close (Table II). It should be noted that the O K-edge XANES spectrum of cassiterite (SnO$_2$), which also crystallizes in the rutile-type structure, exhibits a similar shape as the O K-edge XANES of r-GeO$_2$ and stishovite.[39]

C. Structural analysis

The O K-edge XANES spectrum of q-GeO$_2$ exhibits the peak a, while the O K-edge XANES spectrum of α-quartz does not. Moreover, peak b in the α-quartz spectrum is a preedge shoulder of peak c. We attributed these spectral differences above, to the smaller value of the cation-oxygen-cation angle in the fourfold Ge compound (130° in q-GeO$_2$

and 147.5° in α-quartz). The O K-edge spectrum of K$_2$Ge$_8$O$_{17}$ exhibits features a and b located at the same energy positions as in the q-GeO$_2$ spectrum. Therefore, one expects that the presence of peaks a and b in the O K-edge spectrum of K$_2$Ge$_8$O$_{17}$ is related to similar structural effects.

The crystallographic structure of K$_2$Ge$_8$O$_{17}$ is much more complex than those of α-quartz-like and rutile-type GeO$_2$. The unit cell of K$_2$Ge$_8$O$_{17}$ contains four K$_2$Ge$_8$O$_{17}$ formula units with four nonequivalent Ge sites, two nonequivalent K sites, and 11 nonequivalent O sites. Table III lists the specifics of the 11 oxygen sites in terms of coordination of first neighbor Ge atoms, Ge-O-Ge angle, multiplicity, and Ge-O bond length. The experimental and calculated O K-edge

TABLE III. Oxygen structural atomic environment in K$_2$Ge$_8$O$_{17}$ (from Ref. 22).

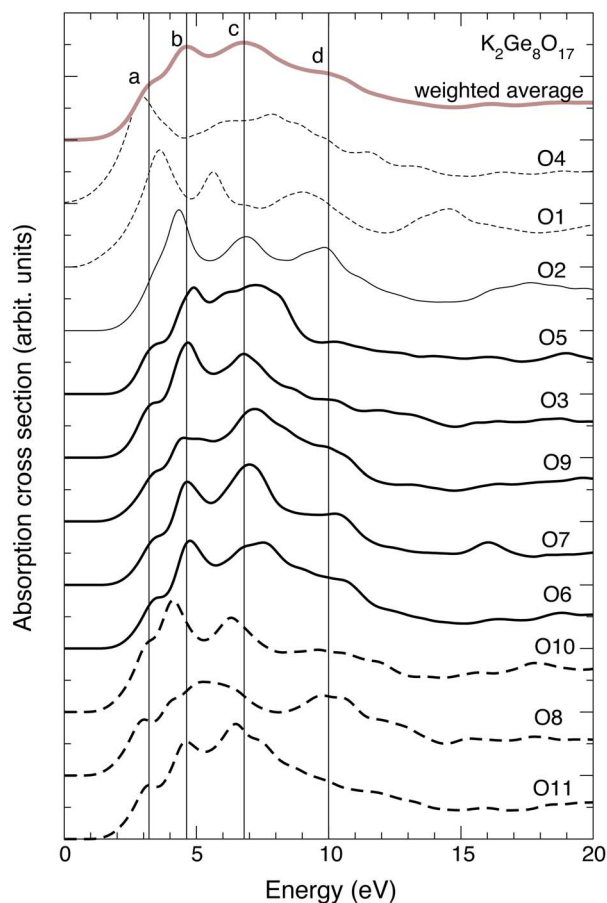| O site	First Ge neighbors	Ge-O bond length (Å)	Ge-O-Ge angle (deg)	Site multiplicity
O4	2 [5]Ge	1.95	91.9	4
O1	2 [5]Ge	1.78	103.4	4
O2	2 [4]Ge	1.75	119.6	4
O5	2 [4]Ge	1.74	129.5	4
O3	2 [4]Ge	1.74	129.7	4
O9	2 [4]Ge	1.74–1.78	131.1	8
O7	2 [4]Ge	1.75–1.75	132.0	8
O6	2 [4]Ge	1.73–1.75	132.6	8
O10	1 [4]Ge	1.74	114.0	8
	1 [5]Ge	1.79		
O8	1 [4]Ge	1.72	126.0	8
	1 [5]Ge	1.84		
O11	1 [4]Ge	1.73	128.6	8
	1 [5]Ge	1.78		

FIG. 5. (Color online) Individual calculated O *K*-edge XANES spectra in $K_2Ge_8O_{17}$. The light solid curve is the weighted average of the eleven contributions. The thin dashed curves correspond to O absorbing atom connected to two fivefold Ge. The solid curves correspond to O absorbing atom connected to two fourfold Ge. The thick dashed curves correspond to O absorbing atom connected to one fourfold Ge and one fivefold Ge.

spectra shown in Fig. 2 are weighted averages of the 11 O absorbing atom sites. Unlike experiment, the calculation provides the 11 individual O *K*-edge XANES spectra. Figure 5 displays the weighted average (as shown in Fig. 2) together with the 11 individual XANES contributions. The individual spectra are all different although some of them exhibit important similarities.

The five O3, O5, O6, O7, and O9 spectra corresponding to oxygen sites connected to two fourfold Ge ([4]Ge) with Ge-O-Ge angle close to 130° are rather similar to the weighted average spectrum and exhibit the a and b features as predicted above by the analysis of the q-GeO$_2$ O *K*-edge spectrum (see the solid thick line curves in Fig. 5). Among these five spectra, the O5 spectrum presents peak b slightly shifted to higher energy, does not clearly exhibit d, and has a very weak peak c. According to Table III, one would expect that the individual spectrum of the O5 site would resemble that of the O3 site. However, one should keep in mind that XANES features are controlled by multiple scattering processes involving not only the coordination shell but also the atomic arrangement at longer distances (medium-range or-

der). The second shell of neighbors of O5 corresponds to six oxygen atoms located around 2.82 Å, followed by two Ge atoms at longer distances (3.66 Å). Conversely, the atomic arrangement of O3 is very different: beyond the two first neighbor fourfold Ge atoms, there are ten oxygen neighbors with distances ranging from 2.75 to 3.54 Å, and then two Ge neighbors at 3.66 Å. The atomic arrangement around O3 is therefore more compact than around O5, thus leading to different spectral signatures especially in the energy range of peaks c and d. The atomic environment of O6, O7, and O9 is also more compact than that of O5.

The O2 oxygen is also connected to two fourfold Ge but with a Ge-O-Ge angle smaller than 130°, i.e., 119.6°. According to the analysis of the electronic structure of q-GeO$_2$, a small Ge-O-Ge angle tends to increase the extent of the Ge s empty states hybridized with O p states. This appears to create features at lower energy from peak c, namely, peaks a and b. In the individual O2 spectrum, peak b is at lower energy than in the individual spectra corresponding to [4]Ge-O-[4]Ge around 130° (O3, O5, O6, O7, and O9), and peak a is then a weak shoulder of peak b.

In the $K_2Ge_8O_{17}$ structure, two O sites are connected to fivefold Ge that are in a distorted trigonal bipyramid geometry (see Fig. 1): O1 with a Ge-O bond length equal to 1.78 Å and Ge-O-Ge of 103.4° (Table III) and O4 with a longer Ge-O bond length (1.95 Å) and smaller Ge-O-Ge angle (91.9°). The corresponding spectra are the thin dashed curves in Fig. 5. The O1 spectrum has a shape very close to that of O2, with all the features shifted to lower energy by about 0.8–1.0 eV. Due to this shift, peaks a and b are not discernable. The shift of features appears to be correlated to the fact that the Ge-O1-Ge angle is smaller than the Ge-O2-Ge angle. In the case of an O connected to two fivefold Ge in trigonal bipyramidal geometry, the Ge-O-Ge angle has to be smaller than in the case of an O connected to two fourfold Ge in tetrahedral geometry. Therefore, the coordination of the Ge neighbors appears to be indirectly related to the shift of the spectral features to lower energy.

The O4 spectrum is very different from all the others. The O4 oxygen is the only oxygen site in the $K_2Ge_8O_{17}$ structure that points into the center of the small four-membered rings (Fig. 1) and has a much longer Ge-O bond length (1.95 Å) than the other oxygens. The O4 spectrum is characterized by a strong peak located at much lower energy than peak a. From the discussion previously, we conclude that the presence of this feature at very low energy is associated with the small value of the Ge-O4-Ge angle (91.9°).

The individual spectra of O8, O10, and O11 (thick dashed curves in Fig. 5) are slightly more difficult to interpret since the absorbing atoms here are connected to one fourfold Ge and one fivefold Ge with Ge-O-Ge angles between 114° and 128.6° (cf. Table III). The three spectra exhibit well-defined a peaks, and exhibit peaks b and c at lower energy than in the resulting weighted average spectrum. The O8, O10, and O11 spectra exhibit the combined effects for the fourfold Ge connected oxygen and for the fivefold Ge connected oxygen that were mentioned above.

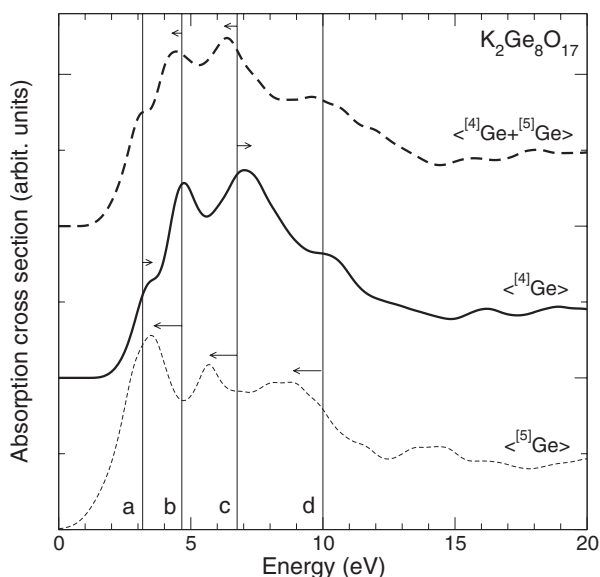In order to better define the fingerprint of O *K*-edge XANES for O connected to two tetrahedral Ge, or to two

FIG. 6. Theoretical O K-edge XANES spectra built from the individual spectra of the oxygen sites of $K_2Ge_8O_{17}$. $\langle^{[4]}Ge+^{[5]}Ge\rangle$ is the mean average of O8, O10, and O11 contributions, $\langle^{[4]}Ge\rangle$ the mean average of O3, O5, O6, O7, and O9, and $\langle^{[5]}Ge\rangle$ the mean average of O1 and O4.

trigonal bipyramidal Ge, or to one of each, we plot in Fig. 6 the mean average of the {O3, O4, O5, O6, O7, and O9} contributions, the {O1 and O4} contributions, and the {O8, O10, and O11} contributions, respectively. These average spectra are, respectively, called $\langle^{[4]}Ge\rangle$, $\langle^{[5]}Ge\rangle$, and $\langle^{[4]}Ge+^{[5]}Ge\rangle$. Figure 6 shows that peaks a–d exhibit energy shifts with respect to their initial positions in the weighted average spectrum. First, the $\langle^{[4]}Ge\rangle$ spectrum exhibits an ~0.3 eV shift to higher energy for features a and c. This is consistent with the relative peak positions observed in the O K-edge XANES spectrum of q-GeO_2 (cf. Fig. 2). Second, the $\langle^{[5]}Ge\rangle$ spectrum exhibits larger shift to lower energy of all the features: for instance, peak c is shifted to lower energy by ~1 eV. Finally, in the $\langle^{[4]}Ge+^{[5]}Ge\rangle$ spectrum, peaks b and c are slightly shifted (~0.3 eV) to lower energy. One common characteristic of the oxygen connected to one or two fivefold Ge is the shift to lower energy of peak c. Such an effect has been previously observed in alkali germanate glasses.[11,12] The −0.4 eV shift of peak c is observable in the Na_2O-GeO_2 and K_2O-GeO_2 (Figs. 8 and 9 of Ref. 11, respectively) at the compositions suggested by the authors to have fivefold Ge present, i.e., at and above the germanate anomaly maximum composition. In Refs. 11 and 12, the authors concluded that a

small shift to lower energy (~0.4 eV) of peak c in the O K-edge XANES spectrum of the alkali germanate glasses was indicative of the formation of five-fold Ge.

V. CONCLUSIONS

We have presented a theoretical analysis of O K-edge XANES spectra of germanate model compounds: rutile-type and α-quartz-like GeO_2, and $K_2Ge_8O_{17}$. Thanks to the *ab initio* framework developed in Ref. 13, the three model compound spectra have been satisfactorily reproduced. For the GeO_2 polymorphs, local DOS calculations have been also performed that permit the interpretation of the various features in terms of orbital hybridization between O p states and Ge s, Ge p, and Ge d states. The presence of peaks a and b in q-GeO_2 and in $K_2Ge_8O_{17}$ appears to be related to Ge-O-Ge angle of about 130° (or less). The value of this angle is strongly correlated to the Ge coordination. We have then shown that the energy and spectral details of the O K edge are influenced by the geometry and electronic state of the Ge environment. The spectrum of $K_2Ge_8O_{17}$ could be interpreted without paying attention to the geometry of the alkali cation. We have demonstrated that the presence of fivefold Ge in the structure leads to a shift toward lower energy of peak c and to a lesser extent of peak b. This result is in agreement with the interpretation of O K-edge spectra of Na_2O-GeO_2 and K_2O-GeO_2 glasses.[11,12] Therefore, this study corroborates the hypothesis that fivefold Ge is involved in the "germanate anomaly" mechanism in Na- and K-bearing germanate glasses. Other germanate structures are under study in order to estimate the effect differing site geometries and coordinations on the O K-edge XANES spectra of alkali containing germanate glasses.

*Electronic address: delphine.cabaret@impmc.jussieu.fr

†Electronic address: henders@geology.utoronto.ca

[1] M. Murthy and J. Ip, Nature (London) **201**, 285286 (1964).

[2] G. S. Henderson and M. E. Fleet, J. Non-Cryst. Solids **134**, 259 (1991).

[3] G. S. Henderson and H. M. Wang, Eur. J. Mineral. **14**, 733 (2002).

[4] M. Ueno, M. Misawa, and K. Suzuki, Physica B & C **120**, 347351 (1983).

[5] C. H. Polsky, K. H. Smith, and G. H. Wolf, J. Non-Cryst. Solids

248, 159168 (1999).

[6] U. Hoppe, R. Kranold, H.-J. Weber, and A. C. Hannon, J. Non-Cryst. Solids **248**, 1 (1999).

[7] G. S. Henderson, J. Non-Cryst. Solids (to be published).

[8] M. Micoulaut, L. Cormier, and G. S. Henderson, J. Phys.: Condens. Matter **18**, R753 (2006).

[9] M. Guthrie, C. A. Tulk, C. J. Benmore, J. Xu, J. L. Yarger, D. D. Klug, J. S. Tse, H-k. Mao, and R. J. Hemley, Phys. Rev. Lett. **93**, 115502 (2004).

[10] G. S. Henderson, X. Liu, and M. E. Fleet, Miner. Mag. **67**, 597607 (2003).

[11] H. M. Wang and G. S. Henderson, Chem. Geol. **213**, 17 (2004).

[12] H. M. Wang and G. S. Henderson, Phys. Chem. Glasses **46**, 377 (2005).

[13] M. Taillefumier, D. Cabaret, A.-M. Flank, and F. Mauri, Phys. Rev. B **66**, 195107 (2002).

[14] D. Cabaret, E. Gaudry, M. Taillefumier, P. Sainctavit, and F. Mauri, Phys. Scr., T **T115**, 131 (2005).

[15] T. Regier, J. Paulsen, G. Wright, I. Coulthard, K. Tan, T. K. Sham, and R. I. R. Blyth, AIP Conf. Proc. **879**, 473 (2007).

[16] W. H. Zachariasen, Z. Kristallogr. **67**, 226 (1928).

[17] G. S. Smith and P. B. Isaacs, Acta Crystallogr. **17**, 842 (1964).

[18] W. H. Baur and A. Khan, Acta Crystallogr., Sect. B: Struct. Crystallogr. Cryst. Chem. **27**, 21332139 (1971).

[19] A. W. Laubengayer and D. S. Morton, J. Am. Ceram. Soc. **54**, 2302 (1932).

[20] T. Yamanaka, T. Fukuda, and J. Tsuchiya, Phys. Chem. Miner. **29**, 633 (2002).

[21] E. Fay, H. Vollenkle, and A. Wittmann, Z. Kristallogr. **138**, 439448 (1973).

[22] B. Harbrecht, J. Kushauer, and H.-J. Weber, Eur. J. Solid State Inorg. Chem. **27**, 831843 (1990).

[23] N. Troullier and J. L. Martins, Phys. Rev. B **43**, 1993 (1991).

[24] L. Kleinman and D. M. Bylander, Phys. Rev. Lett. **48**, 1425 (1982).

[25] R. Haydock, V. Heine, and M. J. Kelly, J. Phys. C **5**, 2845 (1972).

[26] R. Haydock, V. Heine, and M. J. Kelly, J. Phys. C **8**, 2591 (1975).

[27] P. E. Blöchl, Phys. Rev. B **50**, 17953 (1994).

[28] J. Glinnemann, H. E. King, Jr., H. Schulz, T. Han, S. J. La Placa, and F. Dacol, Z. Kristallogr. **198**, 177 (1992).

[29] H. J. Monkhorst and J. D. Pack, Phys. Rev. B **13**, 5188 (1976).

[30] T. Mizoguchi, I. Tanaka, M. Yoshiya, F. Oba, K. Ogasawara, and H. Adachi, Phys. Rev. B **61**, 2180 (2000).

[31] B. Jiang, N. Jiang, and J. Spence, J. Phys.: Condens. Matter **15**, 1299 (2003).

[32] N. Jiang, J. D. Denlinger, and J. Spence, J. Phys.: Condens. Matter **15**, 5523 (2003).

[33] N. Jiang, J. Appl. Phys. **100**, 013703 (2006).

[34] D. M. Christie and J. R. Chelikowsky, Phys. Rev. B **62**, 14703 (2000).

[35] T. Tamura, G.-H. Lu, R. Yamamoto, and M. Kohyama, Phys. Rev. B **69**, 195204 (2004).

[36] S. D. Mo and W. Y. Ching, Appl. Phys. Lett. **78**, 3809 (2001).

[37] T. Sharp, Z. Wu, F. Seifert, B. Poe, M. Doerr, and E. Paris, Phys. Chem. Miner. **23**, 17 (1996).

[38] L. A. J. Garvie, P. Rez, J. R. Alvarez, P. R. Buseck, A. J. Craven, and R. Brydson, Am. Mineral. **85**, 732 (2000).

[39] M. Figueiredo and J. Mirao, Eur. J. Mineral. **14**, 0611067 (2002).

[40] G. Will, M. Bellotto, W. Parrish, and M. Hart, J. Appl. Crystallogr. **21**, 182 (1988).

[41] Calculations were performed with parallel total energy code (PARATEC) by B. Pfrommer, D. Raczkowski, A. Canning, S. G. Louie, F. Mauri, M. Cote, Y. Yoon, Ch. Pickard, and P. Haynes, Lawrence Berkeley National Laboratory (www.nersc.gov/projects/paratec).